# Pre-Swirl Stator and Propeller Design for Varying Operating Conditions

**Saettone, Simone; Regener, Pelle Bo; Andersen, Poul**

*Published in:*
Proceedings of the 13th International Symposium on PRActical Design of Ships and Other Floating Structures (PRADS' 2016)

*Publication date:*
2016

*Document Version*
Peer reviewed version

Proceedings of PRADS2016
4th-8th September, 2016
Copenhagen, Denmark

# Pre-Swirl Stator and Propeller Design for Varying Operating Conditions

Simone Saettone, Pelle Bo Regener, and Poul Andersen

Technical University of Denmark (DTU), Kgs. Lyngby, Denmark

## Abstract

*Over the last two decades, an increasing number of studies have been conducted to develop and improve energy saving devices (ESDs) in order to increase the propulsive efficiency. One well-known example is the pre-swirl stator (PSS), which consists of an often asymmetric arrangement of fixed stator blades ahead of the propeller.*

*This paper describes the hydrodynamic design of a pre-swirl stator with radially variable pitch, paired with a conventional propeller. The aim is to achieve the highest possible efficiency in various operating conditions, and to avoid efficiency penalties in off-design operation.*

*To investigate the propeller and stator designs and configurations in different operating conditions, the computationally inexpensive vortex-lattice method is used as a first step to optimize the geometry in an initial parameter study. Then the flow over hull, stator and propeller is simulated in a CFD-based approach to confirm the results obtained in the first stage.*

## Keywords

Energy Saving Device, Pre-Swirl Stator, Vortex-Lattice Method, RANS-BEM Coupling

## Nomenclature

| | |
|---|---|
| $A$ | panel area |
| $C_f$ | frictional drag coefficient |
| $C_{L,i}$ | ideal lift coefficient |
| $C_{th}$ | thrust loading coefficient |
| $\vec{F}$ | force |
| $H$ | auxiliary function |
| $N_{Ch}$ | number of panels (chordwise) |
| $\vec{R}$ | vector from the vortex element |
| RBC | RANS-BEM Coupling |
| $\vec{U}$ | total velocity |
| $\vec{V}$ | local flow |
| VLM | Vortex-Lattice Method |
| $c$ | chord length |
| $\vec{q}$ | induced velocity with a unit circulation |
| $r$ | radius |
| $s$ | arclength parameter |
| $\vec{u}$ | induced velocity |
| $\vec{x}$ | midpoint of the side |
| $w$ | length of the panel side |

*Greek letters*

| | |
|---|---|
| $\alpha$ | angle of attack |
| $\beta$ | hydrodynamic pitch angle |
| $\Gamma$ | circulation |
| $\gamma$ | chordwise circulation |
| $\kappa$ | weight function |
| $\lambda$ | Lagrange multiplier |
| $\nu$ | ratio of the pressure distribution |
| $\vec{\varepsilon}$ | length element along the panel side |
| $\omega$ | angular velocity |

*Subscripts and Superscripts*

| | |
|---|---|
| 0 | onset flow |
| $FT$ | flat plate pressure distribution |
| $RT$ | rooftop plate pressure distribution |
| $i$ | panel |
| $k$ | panel side |
| $n$ | chordwise panels |
| $m$ | spanwise panels |
| $st$ | stator |
| $pr$ | propeller |
| $r$ | required thrust |
| $t$ | tangential component |
| $tr$ | total required thrust |
| $v$ | skin friction drag |
| $vp$ | skin friction drag propeller |
| $vs$ | skin friction drag stator |

## Introduction

The action of a propeller always involves a loss of energy. This loss can be divided into three main components:

- axial loss,
- rotational loss,
- frictional loss.

The axial loss is inevitable as it comes from the acceleration of the fluid through the propeller disk, which is necessary in order to generate the thrust. The frictional loss is due to the friction generated by the water that gets in contact with the surface of the propeller blade. The surface's roughness, the total surface area of the blade and the speed of rotation are the dominating factors in frictional losses. The rotation of the blades causes a rotation in the wake and, as a consequence, this leads to a

loss of energy: the rotational loss. Pre-swirl stators (PSS) aim at reducing or recovering rotational energy losses by generating a swirling flow opposite to the sense of the rotation of the propeller. They also have a simple shafting system, considerable efficiency gain (3-8% according to Shin et al., 2015), a relatively low initial cost of installation as well as high reliability. This device modifies the loading of the propeller blades, through which the delivered thrust per unit of power is raised.

In the present study, the hydrodynamic design of a pre-swirl stator with variable pitch, paired with a conventional propeller, is investigated. First, this design problem is approached by seeking the optimum distribution of circulation along the different components of the propulsion system. More specifically, a variational problem is solved where the propeller torque is minimized for a given total thrust. The approach used is similar to the classic theory, where the propeller is modeled as a lifting line and the continuous distribution of circulation is discretized. However, in this case, the propeller and the stator are modeled by employing the vortex-lattice method (VLM) to obtain a better representation of the flow. Afterwards, a RANS-based approach is used to confirm the results obtained by the VLM. In this method, the propeller effect is modeled through body forces that are computed by an unsteady boundary-element (BEM) code.

## Vortex-Lattice Method

A variational problem is solved in order to find the optimum radial distribution of circulation on the stator and the propeller, which provides the highest propulsive efficiency. Prandtl and Betz (1927) were the first to solve this problem for a single propeller in open water conditions. Later, Lerbs (1952) developed a method which included a radially varying onset flow. Kerwin et al. (1986) introduced a new approach where the continuous distribution of circulation was discretized, which makes it possible to solve the variational problem directly. Coney (1992) developed a vortex-lattice lifting line method where, again, the continuous distribution of vortices along the lifting-line is discretized. These two last works showed an important advantage of the discrete model: the propeller geometry can be theoretically unlimited complex. The present optimization procedure employs a lifting-surface model for both propeller and stator, which makes it possible to include the effects of the entire blade in the optimization. The presence of the hub is ignored.

### *Grid Generation*

The blade surface is divided into quadrilateral panels as the continuous distribution of circulation is replaced with a discrete distribution. The spanwise discretization for both propeller and stator is in accordance with James (1972). Meanwhile, the chordwise discretization is in accordance with James (ibid.) for the stator and with Lan (1974) for the propeller.

The trailing vortex sheet is, due to the discretization, reduced to a finite number of horseshoe vortices, which is a simplified representation of the vortex system of a wing. The horseshoe vortex consists of two trailing vortices, which are aligned infinitely downstream with the fluid, and a bound vortex, which is a straight line located at the trailing edge. The circulation of the horseshoe vortex is equal to the circulation of the adjacent trailing edge panel (Kutta condition). The sides of the horseshoe for the propeller are assumed to follow regular helices with constant pitch and radius. On the other hand, the wake of the stator is divided into two parts:

- Straight line vortices aligned with the surface of the stator
- Straight line vortices perpendicular to the propeller plane

The length of these two wakes of the stator depends on its configuration and on the operational condition.

### *Forces and Velocities*

The force on a panel side is found from the Kutta–Joukowski theorem:

$$\vec{F}_k = \rho \vec{U}(\vec{x}) \times \vec{\Gamma}_k \tag{1}$$

The total forces generated by each component are found using the contribution from all the panel sides. The total velocity $\vec{U}(\vec{x})$ is the sum of the onset flow, the induced velocity from the component itself and the circumferential mean induced velocity from the other component. The onset flow is assumed to be independent of the longitudinal position and axisymmetric, therefore the onset flow only varies radially. The induced velocity from the panels is found using the Biot-Savart law, so that the effects of the skew and the skew induced rake are taken into account. Hence, the velocity induced by one panel in the point $\vec{x}$ is:

$$\vec{u}_i(\vec{x}) = \frac{\Gamma_i}{4\pi} \sum_{k=1}^{4} \int_0^{w_k} \frac{d\vec{\varepsilon} \times \vec{R}}{|\vec{R}|^3} = \Gamma_i \vec{q}_i(\vec{x}) \tag{2}$$

The induced velocity from the horseshoe vortices of the propeller is divided into two parts: the transition wake and the ultimate wake. The transition wake covers the helix from the trailing edge of the propeller to four radii downstream. The regular helix in the transition wake is replaced by a number of straight line vortices. Thus, the induced velocity is found in the same way as for the panel side. The ultimate wake covers the part from the end of the transition wake to infinity downstream. The induced velocity is found by the method developed by de Jong (1991). The induced velocity from the wake of the stator is found in the same way as for the panel side.

### *Weight Function*

A weight function is introduced to specify the chordwise distribution of circulation for both components. As a consequence, the optimization problem is reduced to finding

the optimum distribution of the total circulation for each chordwise strip, which corresponds to the circulation of the horseshoe vortex. Therefore, the number of unknown circulations corresponds to the total number of spanwise panels of the components. The weight function is:

$$\kappa_n = \sum_{i=n+1}^{N_{Ch+1}} \left( (1-\nu)\,\kappa_i^{RT} + \nu \kappa_i^{FT} \right) \tag{3}$$

The distribution of circulation related to the angle of attack corresponds to the distribution for a flat plate with an angle of attack (Breslin and Andersen, 1994):

$$\gamma_{FP}(x) = 2U_0\,\alpha \sqrt{\frac{c/2+x}{c/2-x}} \tag{4}$$

The distribution of circulation related to the camber line is (Breslin and Andersen, 1994):

$$\gamma_{RT}(x) = \begin{cases} \frac{(c/2+x)U_0}{c\left(1-a^2\right)} C_{L,i} & \text{if} \quad x \le c/2\,(1-2a) \\ \frac{U_0}{1+a} C_{L,i} & \text{if} \quad c/2\,(1-2a) \le x \end{cases} \tag{5}$$

The ratio of the pressure distribution $\nu$ is set 0 for the propeller (pure rooftop) and 1 for the stator (pure flat-plate).

### *Grid Alignment*

The surface of each component has to be parallel to the total velocity $\vec{U}(\vec{x})$. The applied grid alignment procedure assumes that the pitch of the shed vortices is constant on the surface of each component. The pitch is based on the total velocity at the mid-chord line of the blade. Therefore, the pitch angle for the propeller is:

$$\beta_{pr} = \tan^{-1}\left( \frac{U_{0,x}(s) - u_x(s)}{\omega r_m - u_t(s) - U_{0,t}(s)} \right) \tag{6}$$

Whereas, the pitch angle for the stator is:

$$\beta_{st} = \tan^{-1}\left( \frac{U_{0,x}(s) - u_x(s)}{-u_t(s) - U_{0,t}(s)} \right) \tag{7}$$

It is worth mentioning that this grid alignment leads to a twisted stator at the end of the optimization procedure.

### *Wake Alignment*

The free vortex elements must be parallel to the local flow direction in order not to generate force in the fluid:

$$\vec{V} \times \vec{\Gamma}_{wake} = 0 \tag{8}$$

The implemented wake alignment procedure neglects the contraction of the slipstream and assumes that the pitch of the horseshoe vortices is constant. The pitch angle of the horseshoe vortices of the propeller is set equal to the fluid pitch angle of the propeller $\beta_{pr}$. Regarding the stator, the wake is divided into two parts, as mentioned on the previous page.

### *Skin Friction Drag*

The skin friction drag is the part of the drag created in the boundary layer due to the viscosity of the water. This force is taken into account by using a frictional drag coefficient $C_f$, which is estimated on the basis of experiments (Breslin and Andersen, 1994). Here, the skin friction drag of a panel is taken as:

$$dT_v = \frac{1}{2}\,\rho\, C_f\, A\, |U_t|\, U_t \tag{9}$$

### *Variational Iteration Problem*

A thorough explanation of the variational iteration problem is given by Coney (1992). In this section just a brief description is given. The distribution of circulation for both components is found by using a variational approach based on the method of Lagrange multipliers. The auxiliary function $H$ is:

$$H\left(\vec{\Gamma}, \lambda\right) = \omega Q\left(\vec{\Gamma}\right) + \lambda\left(T_{pr}\left(\vec{\Gamma}\right) + T_{st}\left(\vec{\Gamma}\right) - T_{tr}\right) \tag{10}$$

Where:

$$T_{tr} = T_r - T_{vp} - T_{vs} \tag{11}$$

It is worth pointing out that it is necessary to compute the circulation for each blade of the stator as it is usually not symmetric (and not only for one blade as it is performed for the propeller). The optimum distribution of circulation is found by setting the partial derivatives of $H$, with respect to $\vec{\Gamma}$ and $\lambda$, to zero:

$$\frac{\partial H}{\partial \Gamma_m} = 0 \qquad \frac{\partial H}{\partial \lambda} = 0 \tag{12}$$

This optimization procedure is non-linear and, therefore, equations (12) are replaced with a linear system of equations. Iterations are necessary to achieve a solution to the problem. The distribution of circulation is initially set to zero and the Lagrange multiplier to -1 (Coney, 1992) and the system is solved. At this point, a new distribution of circulation and a new Lagrange multiplier are found and the system is solved again. The iteration for the variational problem is continued until convergence is achieved, which is normally reached after less than ten iterations. Then the wake is aligned with the local flow direction and the grids are reconstructed. Thereupon, the system of equations is updated with the new grids, new wake geometry and new skin friction drag, for both propeller and stator, and the problem is solved again. The alignment of the grids and the wake is continued until convergence is achieved. It is necessary to obtain the optimum distribution of circulation without changing either wake or grids. Therefore, the induced velocities are fixed during the circulation optimization procedure since they are exclusively functions of the component's geometry.

## RANS-BEM Coupling

Originally introduced by Stern et al. (1988), using a viscous flow solver for the flow around the hull and coupling it with a potential flow-based method for the propeller is an efficient tool to including the propeller effect

in a CFD simulation. Over the last years, this approach has gained popularity even though unsteady and fully viscous simulations with a discretized propeller are possible today. This is not only due to the vastly reduced computational effort, but also as the coupled method allows for analyzing details of the hull-propeller interaction, as the effective wake field is computed explicitly. As RANS-based simulations can be carried out in both model and full scale, this hybrid (coupling) method can also be used to study different scale effects, including scaling of effective wake fields (Starke and Bosschers, 2012).

Potential flow-based tools for propeller analysis, such as panel codes (boundary element method, BEM), are of course not able to capture and resolve all flow features and details due to the simplifications made. Still, the propeller's global unsteady forces – and therefore its effect – can be predicted with good accuracy. This is taken advantage of in a RANS-BEM coupling (RBC) method, where the flow around the propeller is computed in a panel method while the flow around the hull is resolved by RANS. To further reduce the computational effort, this study treats the hull flow as a steady-state problem and the unsteady propeller forces are time-averaged before being added as momentum sources to the RANS computation. As the inflow to the propeller changes as the simulation progresses, this coupling is of iterative nature. The velocity field in the coupling plane is passed from the RANS solver to the propeller program, which then returns the updated time-averaged forces that correspond to this new inflow field.

As the velocities extracted from the RANS part do not directly correspond to the propeller inflow field, but represent the *total* velocity wake field including the propeller-induced velocities, the induced velocity field from the previous iteration is subtracted from the *total* wake field to estimate the *effective* wake field.

Technically, these velocities can be computed and exchanged in an arbitrary location. However, both robustness and accuracy depend strongly on the location of this *coupling plane*. Ideally, one would want to place the coupling plane in the propeller plane or the blade-midchord plane, but the presence of singularities on the blade surface in the BEM make it difficult or impossible to evaluate the induced velocities in these locations.

The simplest solution is to use a single plane upstream of the propeller as the coupling plane. Yet, a number of more advanced options exist (see e.g. Rijpkema et al., 2013), such as using curved upstream surfaces or multiple planes for extrapolation. In the present study, the effective wake is computed on a curved surface that follows the blade leading edge contour closely, essentially resulting in a single, curved upstream coupling plane as also described by Tian et al. (2014). The absolute result values could possibly be improved by using a correction factor approach as suggested by Sánchez-Caja et al. (2014), but as the correct prediction of trends is more important than matching certain exact values for this design and optimization task, no "corrections" – that might even obfuscate unexpected effects or mistakes – are applied.

In this project, the XCHAP solver from the commercial SHIPFLOW package is used on the RANS side, while the propeller flow and forces are computed by the DTU-developed panel code called ESPPRO. XCHAP uses structured, overlapping grids and the EASM (Explicit Algebraic Stress Model) turbulence model. A separate cylindrical propeller grid is used for easy transfer of propeller forces while fully conserving thrust and torque.

## Results – Open Water (VLM)

### *Effect of the Stator on the Propeller*

First, different types of propeller and stator designs are investigated in order to explain the overall effect of the stator on the propeller. The general trend of this analysis is shown in the following example. The stator has a simple configuration with 4 blades and constant chord length. The propeller adopted is the DTNSRDC 4381 (Carlton, 2012). Propeller and stator have the same diameter and they both see uniform flow. Their axial distance is set to 0.5R. However, it is worth pointing out that since the contraction of the slipstream is ignored, the effect of the distance between the stator and the propeller on the efficiency is negligible (Glover, 1991). The design point is:

$$J = 0.952, \quad C_{Th} = 0.604$$

Figure 1 shows the optimum circulation for both the two components and the same propeller under identical operation conditions. The stator circulation and that of the propeller have opposing signs. The stator increases the efficiency by modifying the distribution of circulation on the propeller: it decreases, gets flatter and moves toward the propeller root. This is due to the swirl induced by the stator that reduces the downstream tangential velocities generated by the propeller (Fig. 2). It is important to note that the propulsive efficiency increases even though the stator generates drag rather than thrust. These results are in agreement with Coney (1992). This investigation also shows that the stator influences the propeller by reducing its optimum pitch angle $\beta_{pr}$ (Fig. 3): this is due to the

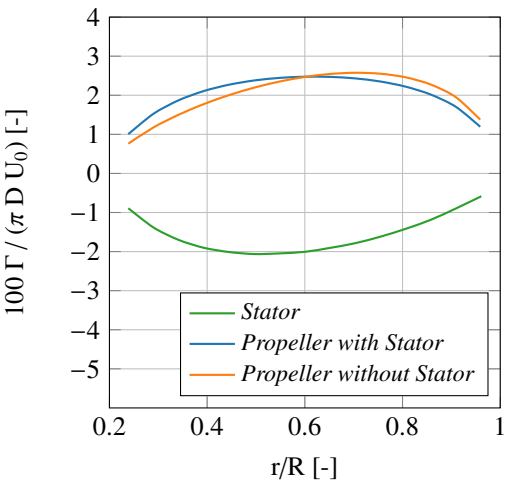


**Figure 1.** Optimum radial circulation distribution for propeller and pre-swirl stator

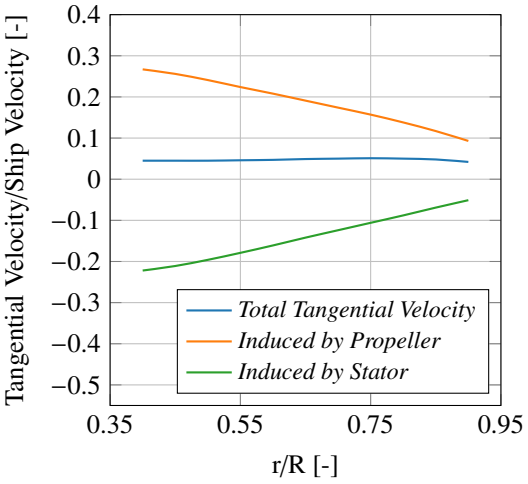


**Figure 2.** Circumferential mean tangential velocities induced $0.5R$ downstream by propeller/stator combination

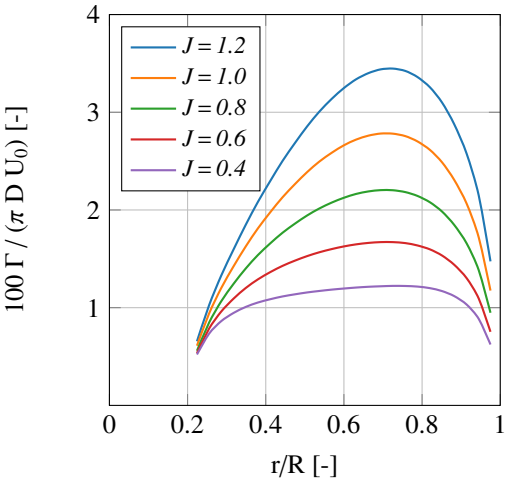


**Figure 4.** Optimum radial circulation distribution for a free-running propeller for varying values of J

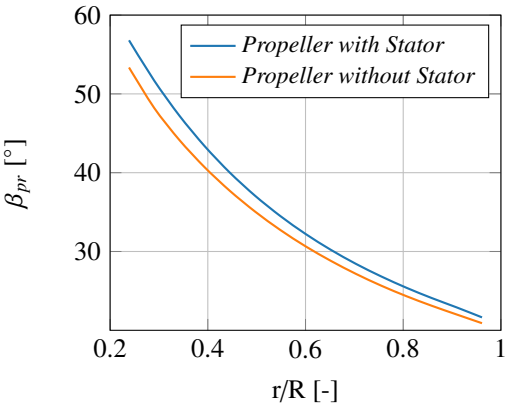


**Figure 3.** Optimum pitch angle $\beta_{pr}$ distribution for propeller with and without pre-swirl stator

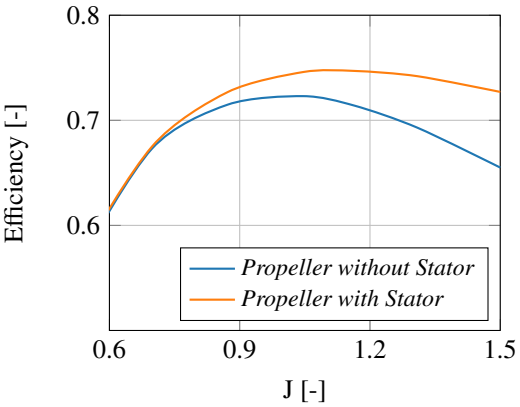


**Figure 5.** Efficiency with and without stator for different values of angular velocity

reduction of the total tangential induced velocities $u_t$.

It is worth pointing out that the comparison between the optimization of the propeller with and without the influence of the stator is performed by keeping constant:

- The required thrust of the propeller $T_r$
- The rate of revolutions of the propeller $n$
- The mean velocity to the propeller disc $U_a$

In other words, the stator's presence influences the optimum distribution of radial circulation on the propeller by providing a lower value of the total torque, while $T_r$, $n$ and $U_a$ remain the same.

The function of the stator as a device that induces tangential velocity to the propeller can easily be demonstrated. The analysis is performed for the propeller alone with constant ship velocity and required thrust. The advance ratio is varied as a consequence of varying angular velocity of the propeller. The design point is:

$$U_0 = 10\ m/s, C_{Th} = 0.604$$

Figure 4 shows two results:

- The bigger the angular velocity $\omega$ (onset flow), the flatter the curve
- The bigger the angular velocity $\omega$ (onset flow), the more the load moves out toward the propeller tip

These results are analogous to those shown in Fig.1, where the stator induces tangential velocity corresponding to the change in angular velocity in Fig. 4.

### *Operational Conditions Parameters*

The next point of the investigation implies the variation of the angular velocity and the required thrust to obtain a better insight in the effect of the stator in different operating conditions.

*Angular Velocity*

The angular velocity $\omega$ of the propeller is varied from 7 to 15 rad/s while the other parameters are kept constant. Different types of propeller and stator designs are investigated and the general trend of this analysis is shown in the following example. The stator has a simple configuration with 4 blades and constant chord length. The propeller adopted is the DTNSRDC 4381 (Carlton, 2012). Propeller and stator have the same diameter and they both see uniform flow. Their axial distance is set equal to 0.5R.

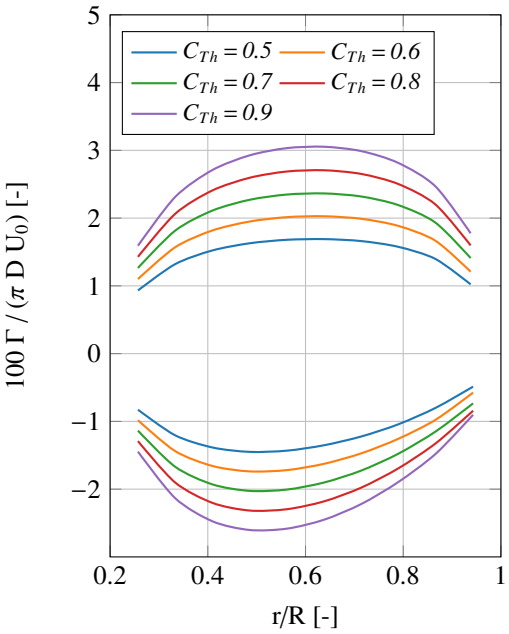


**Figure 6.** Optimum radial circulation distribution for a free-running propeller for varying values of J

The design point is:

$$U_0 = 10\ m/s, \quad C_{Th} = 0.662$$

Fig. 5 shows the gain in efficiency against the angular velocity of the propeller. It can be seen that the efficiency gets higher with the decreasing of $\omega$. To explain these results it is necessary to imagine a range of identical propellers working with the same value of required thrust $T_r$ and mean inflow to the propeller disc $U_a$ but with a different value of angular velocity $\omega$. In this hypothetical situation two concepts are fundamental:

- if the propeller is working with a high angular velocity, the required thrust is generated by high velocities and small circulations on the propeller,
- if the propeller is working with a small angular velocity, the required thrust is generated by small velocities and high circulations on the propeller.

Therefore, the stator has a much bigger impact on the propeller when the angular velocity is low because the velocities induced on the propeller by the stator are relatively larger for low angular velocities.

*Required Thrust*

The thrust loading coefficient $C_{th}$ is varied from 0.5 to 0.9 while the other parameters are kept constant. As already performed for the previous investigations, different types of propeller and stator designs are investigated and the general trend of this analysis is shown in the following example. The set-up implemented for both propeller and stator is the same as the one adopted for the angular velocity. The design point is:

$$U_0 = 10\ m/s, \quad J = 0.8$$

The investigation shows that the gain in efficiency is higher with the increasing of the thrust loading coefficient $C_{th}$. Figure 6 shows the optimum distribution of circulation for propeller (positive) and stator (negative) for different thrust loading coefficients.

From this, an important result can be seen: the higher the required thrust, the higher the absolute value of circulation. As a consequence, the stator has a much bigger impact on the propeller when $C_{th}$ is high because the velocities induced on the propeller by the stator are higher.

These two last investigations also show that the optimum geometry for both components changes depending on the operation condition. Considering the stator, the higher the absolute value of circulation on the stator the more the optimum stator geometry is twisted.

## Results – Behind Ship Condition (VLM/RBC)

The previous section gives some insight into the general working principle of pre-swirl stators. It also shows general trends and findings from running vortex lattice-based optimizations for propellers and stators. In this section, both previously introduced methods – VLM and RANS-BEM coupling – are used to also investigate the performance of propeller-stator configurations in the behind ship condition, including off-design operating conditions. This particular implementation of the VLM cannot be used to analyze a given geometry, but will always find the optimum circulation to minimize the torque for a required thrust, thereby finding the optimum geometry. For this reason, results for the off-design conditions are only provided by the RBC approach.

**Case and Configuration** For this case study, the KCS case (Kim et al., 2001) is used, representing a typical container ship design from the late 1990s. The first operating condition considered corresponds to the design point of KCS. A second condition is created by lowering the thrust requirement by 40%, the floating position and all other parameters being identical to the first condition. All optimizations and simulations are carried out in full scale. These conditions have been selected to obtain two sufficiently different, yet representative conditions for the propulsion system with reasonable simulation effort.

The propeller design is based on the KCS stock propeller (Kim et al., 2001), where pitch and camber distributions are replaced by the VLM results. To further simplify the blade geometry, skew is removed.

A common asymmetric, four-blade configuration is chosen for the stator: three blades on the port side and one on the starboard side. This is the standard configuration adopted for a wide range of vessels (bulk carriers, container ships, tankers, etc). The chord length is assumed to be 1.5 m at the root and 0.9 m at the tip. Propeller and stator have the same diameter. The axial distance between propeller leading edge and stator trailing edge is 2.0 m.

**VLM Setup** First, the VLM is used to find an optimum propeller/stator configuration for condition 1 (Case 1, see Tab. 1) and for condition 2 (Case 4, see Tab. 2). Propeller P1 and stator S1 are therefore the result of the optimization for condition 1, whereas P2 and S2 correspond to condition 2. Note that the two components – propeller

**Table 1.** Simulations for Condition 1

| Case ID | Propeller | Stator | $\Delta P_{D,\mathrm{VLM}}$ | $\Delta P_{D,\mathrm{RBC}}$ |
|---|---|---|---|---|
| Case 1 | P1 | S1 | -4.6 % | -7.1 % |
| Case 2 | P1 | S2 | — | -6.4 % |
| Case 3 | N1 | — | 0.0 % | 0.0 % |

**Table 2.** Simulations for Condition 2

| Case ID | Propeller | Stator | $\Delta P_{D,\mathrm{VLM}}$ | $\Delta P_{D,\mathrm{RBC}}$ |
|---|---|---|---|---|
| Case 4 | P2 | S2 | -5.2 % | -4.9 % |
| Case 5 | P2 | S1 | — | -4.5 % |
| Case 6 | N2 | — | 0.0 % | 0.0 % |

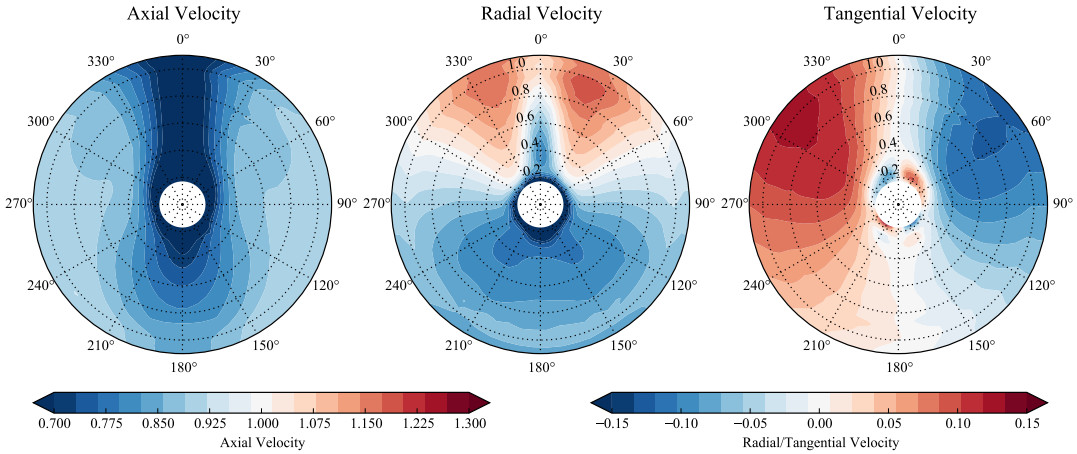


**Figure 7.** Effective wake for the full scale KCS case without stator

and stator – are always optimized together.

To evaluate the power reduction associated with the pre-swirl stators, a reference propeller is designed for each condition using the same optimization method, just run without stators (those propellers are called N1 and N2). All components are optimized for the wake field shown in Fig. 7, which is the effective wake field in condition 1 with the KCS stock propeller, as obtained by the RANS-BEM coupling approach. The change in effective inflow due to a redesigned (optimized) propeller was checked and turned out to be negligible. For the steady-state VLM propeller optimization, this wake field is averaged circumferentially, yet the correct angular positions for the stator blades are taken into account.

**RBC Setup** On the RANS side, a global, body-fitted and symmetric background grid is created around the unappended hull (H-O topology) using SHIPFLOW's XGRID grid generator. It extends one ship length both upstream and downstream of the forward and aft perpendicular, respectively. The stator blades are added as separate grids (C-O topology) that are fitted to the hull at the blade root and stretched towards all noslip boundaries including the hull. The target $y^+$ value when stretching grids is 0.7.

The total number of cells including refinement grids in the aftbody region then amounts to about 14 million, but given that the grids are of structured type and many of the cells are interpolation cells, the required CPU time for solving is still very reasonable. Running on 40 CPUs, the solution converges after about 2 hours of wall clock time.

**Result Evaluation** For the off-design cases, the propeller speed is modified iteratively to reach the required thrust for the respective condition. For Case 2, the propeller speed increases (compared to Case 1), as the stator S2 provides less pre-swirl than S1, and propeller P1 was designed to operate together with stator S1. The opposite effect is seen in Case 5 (relative to Case 4). The difference in the pre-swirl created by the two stators can be seen from Fig. 8, which shows the tangential components of the effective wake field for the two stators.

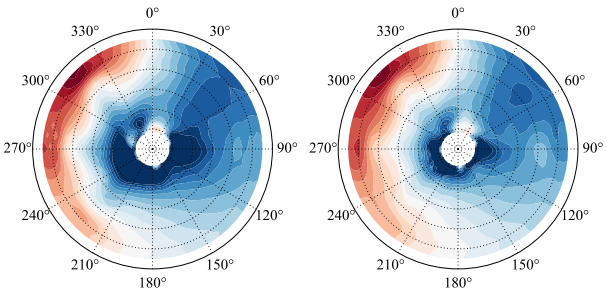

**(a)** Case 1 **(b)** Case 2

**Figure 8.** Effective tangential velocities

As all cases correspond to the same ship speed, but different propeller thrusts (due to the stator's drag), they are evaluated based on the delivered power $P_D = 2\pi nQ$. Tables 1 and 2 show the reduction in power for all cases with a pre-swirl stator compared to the stator-less configuration. The tables show the values predicted by both the Vortex-Lattice Method (VLM) and the RANS-BEM coupling (RBC).

**Discussion** Tables 1 and 2 show that the optimized propeller/stator configuration from the VLM gives a higher power reduction than using the stator optimized for the other condition in an off-design scenario.

It should be noted, however, that the efficiency gain for Condition 2 (1.7%) is significantly lower than for Condition 1 (3.8%), due to the lower propeller loading. This is perfectly in line with the theory outlined earlier. Still, the

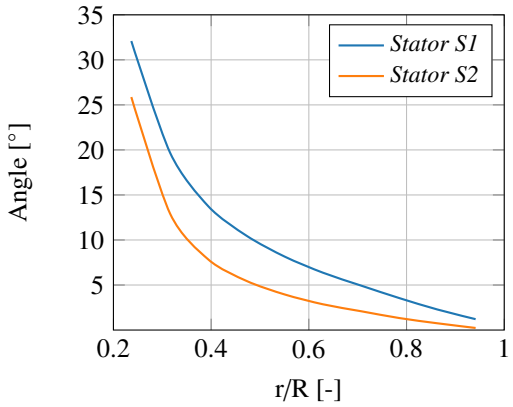


**Figure 9.** Geometric angle of blade at 225° position

relative power reduction is of similar magnitude for both conditions.

With respect to stator geometry, the difference in the geometric pitch angle of a stator optimized for Condition 1 and a stator optimized for Condition 2 can be seen from Fig. 9 and is in the order of 2-5°. However, it should be noted that the difference varies with the radius, with the pitch angle at the tip being very similar. This poses additional practical challenges to the concept of controllable pitch pre-swirl stator blades.

Also, a stator optimized for a different condition still provides considerable power savings compared to the stator-less configuration, indicating that the global effect is not very sensitive to the stator pitch angle in the interval of operating conditions that was looked at.

## Conclusions

From the results presented in the previous sections it can be concluded that:

- the simple Vortex-Lattice model can be used to design both propellers and pre-swirl stators and also gives a good indication of efficiency gains and power savings,
- a pre-swirl stator designed for one condition can also perform fairly well in an off-design condition, suggesting a "flat" optimum.

## Acknowledgement

The work was supported by Innovation Fund Denmark and the Danish Maritime Fund under the Blue INNOship partnership.

## References

Breslin, J. P. and Andersen, P. (1994). *Hydrodynamics of Ship Propellers*. Cambridge University Press.

Carlton, J. (2012). *Marine Propellers and Propulsion*. Butterworth-Heinemann, Oxford.

Coney, W. B. (1992). Optimum Circulation Distributions for a Class of Marine Propulsors. *Journal of Ship Research*, 36(3):210–222.

de Jong, K. (1991). *On the optimization and the design of ship screw propellers with and without end plates*. PhD thesis, University of Groningen.

Glover (1991). Rotor/Stator Propulsors - Parametric Studies. In *Hydronav'91*, Gdańsk-Sarnówek.

James, R. M. (1972). On The Remarkable Accuracy Of The Vortex Lattice Method. *Computer Methods in Applied Mechanics and Engineering*, 1(1):59–79.

Kerwin, J. E., Coney, W. B., and Hsin, C.-Y. (1986). Optimum Circulation Distribution for Single and Multicomponent Propulsors. *21st American Towing Tank Conference*, pages 53–62.

Kim, W. J., Van, S. H., and Kim, D. H. (2001). Measurement of flows around modern commercial ship models. *Experiments in Fluids*, 31(5):567–578.

Lan, C. E. (1974). A quasi-vortex-lattice method in thin wing theory. *Journal of Aircraft*, 11(9):518–527.

Lerbs, H. W. (1952). Moderately Loaded Propellers with a Finite Number of Blades and an Arbitrary Distribution of Circulation. *SNAME Transactions*, 60:73–117.

Prandtl, L. and Betz, A. (1927). *Vier Abhandlungen zur Hydrodynamik und Aerodynamik*. Kaiser Wilhelm Institut für Strömungsforschung, Göttingen.

Rijpkema, D., Starke, B., and Bosschers, J. (2013). Numerical simulation of propeller-hull interaction and determination of the effective wake field using a hybrid RANS-BEM approach. In *3rd International Symposium on Marine Propulsors (smp'13)*, pages 421–429, Launceston, Australia.

Sánchez-Caja, A., Martio, J., Saisto, I., and Siikonen, T. (2014). On the enhancement of coupling potential flow models to RANS solvers for the prediction of propeller effective wakes. *Journal of Marine Science and Technology*, 20(1):104–117.

Shin, Y.-J., Kim, M.-C., Lee, W.-J., Lee, K.-W., and Lee, J.-H. (2015). Numerical and Experimental Investigation of Performance of the Asymmetric Pre-Swirl Stator for the Container Ship. In *4th International Symposium on Marine Propulsors (smp'15)*, Austin, TX.

Starke, B. and Bosschers, J. (2012). Analysis of scale effects in ship powering performance using a hybrid RANS-BEM approach. In *29th Symposium on Naval Hydrodynamics*, pages 26–31, Gothenburg, Sweden.

Stern, F., Kim, H., Patel, V., and Chen, H. (1988). A Viscous-Flow Approach to the Computation of Propeller-Hull Interaction. *Journal of Ship Research*, 32(4):246–262.

Tian, Y., Jeon, C.-H., and Kinnas, S. A. (2014). On the Accurate Calculation of Effective Wake/Application to Ducted Propellers. *Journal of Ship Research*, 58(2):70–82.